Received: 23 April 2017 | Revised: 29 June 2017 | Accepted: 18 July 2017

DOI: 10.1002/gj.3004

WILEY

SPECIAL ISSUE ARTICLE

In situ LA-ICP-MS trace element analysis of magnetite from the late Neoarchean Gongchangling BIFs, NE China: Constraints on the genesis of high-grade iron ore

Xiaohui Sun[1,2] | Xiaoqing Zhu[2] | Haoshu Tang[2] | Yan Luan[1]

[1] School of Earth Science and Resources, Chang'an University, Xi'an, China

[2] State Key Laboratory of Ore Deposit Geochemistry, Institute of Geochemistry, Chinese Academy of Sciences, Guiyang, China

Correspondence
Xiaohui Sun, School of Earth Science and Resources, Chang'an University, Xi'an 710054, China.
Email: sunxiaohui@chd.edu.cn

Haoshu Tang, State Key Laboratory of Ore Deposit Geochemistry, Institute of Geochemistry, Chinese Academy of Sciences, Guiyang 550081, China.
Email: tanghaoshu@163.com

Funding information
National Natural Science Foundation of China, Grant/Award Number: 41503035 and 41672086; Major State Basic Research Program of China, Grant/Award Number: 2012CB416602; Natural Science Basic Research Plan in Shaanxi Province of China, Grant/Award Number: 2017JM4006 and 2016JQ4010; Fundamental Research Funds for the Central Universities, Grant/Award Number: 310827151060 and 310827161007

Handling Editor: G. Yang

The Precambrian banded iron formations (BIFs) not only relate to the evolution of life, ocean, and atmosphere but also provide important reserves of iron around the world. The Gongchangling iron ore deposit located in the Anshan-Benxi area of Liaoning Province, China, is oxide facies Algoma-type BIFs, and the Gongchangling No.2 mining area is famous for the production of high-grade iron ore in China. Magnetite is the main ore mineral in the Gongchangling iron ore deposit, and the magnetite mainly exhibits three modes of occurrence: BIFs (without actinolite), actinolite-bearing BIFs, and high-grade iron ore. Trace elemental compositions of the magnetite with different occurrences of the Gongchangling iron ore deposit were obtained by laser ablation inductively coupled plasma mass spectrometry to constrain the genesis of the high-grade iron ore. The magnetite from actinolite-bearing BIFs shows relatively lower contents of Mg, Al, Mn, and Zn compared to the magnetite from BIFs (without actinolite), suggesting that coexisting minerals have played an important role in the trace element concentration in magnetite. The magnetite from high-grade iron ore has lower contents of Ti and V and higher contents of Al and Mn than counterpart from BIFs (with/without actinolite), indicating that the high-grade iron ore may be reformed by high temperature metamorphic hydrothermal fluid. The staurolite-garnet-biotite schist is the wall-rock of high-grade iron ore, and the garnet-biotite geothermometry is used to evaluate the metamorphic temperature of 593 ± 17 °C. It is proposed that the metamorphic hydrothermal fluid produced during regional metamorphism reformed BIFs to generate high-grade iron ore.

KEYWORDS

banded iron formations, geothermometry, LA-ICP-MS, magnetite, North China Craton, trace element

1 | INTRODUCTION

The banded iron formations (BIFs), as a unique product in the Precambrian, are alternating layers of iron-rich and silicon-rich chemical precipitates (Gross, 1980; James, 1954). Based on the mineralogical assemblage and tectonic setting, the BIFs are classified into Algoma-type, associated with volcanic rocks, and Superior-type strata-bound in sedimentary sequences (Gross, 1980). The BIFs constitute the most important type for iron resources in the world; moreover, the deposition of BIFs is linked to environmental and geochemical evolution of the early Earth (Bekker et al., 2010). Therefore, research on BIFs not only has great economic significance but also plays a considerable role in understanding the evolution of the atmosphere and biosphere, as well as coeval ocean composition.

In China, the BIFs are widely distributed in the North China Craton (NCC), including the western Liaoning, eastern Hebei, middle Inner Mongolia, northern Shanxi, western Anhui, south-western Henan, and the western Shandong provinces (Wan et al., 2012; Zhang, Zhai, Wan et al., 2012a; Zhang, Zhai, Zhang et al., 2012b). In the NCC, the Archean Algoma-type BIFs are dominant, and the superior-type BIFs formed during the Paleoproterozoic occur subordinately, which strongly contrast with distribution features of BIFs around the world (Li et al., 2014; Zhai & Windley, 1990).

The Gongchangling iron deposit, oxide facies Algoma-type BIFs in the Anshan-Benxi area of Liaoning Province, is famous for the

production of high-grade iron ore in the Gongchangling No.2 mining area in China (Zhou, 1987, 1994, 1997). However, as for the genesis of high-grade iron ore, there are still highly different viewpoints, including the following: (a) original deposition mechanism (Chen et al., 1984); (b) hydrothermal reformation mechanism. However, there are two distinctively different opinions on the nature of the hydrothermal fluid, including migmatitic hydrothermal fluid from magma (Chen et al., 1985; Cheng, 1957; Li, Li, Cui, & Wang, 1977; Li et al., 2012; Zhao & Li, 1980; Zhao, Wang, & Li, 1979) and metamorphic hydrothermal fluid generated during regional metamorphism (Guan, 1961; Li & Shi, 1979; Liu & Jin, 2010; Shi & Li, 1980; Sun, Zhu, Tang, Zhang, & Luo, 2014; Wang, Xia, Fu, Jia, & Men, 2014; Zhou, 1994); and (c) the graphite-bearing high-grade iron ore was formed by decomposition of siderite during epidote–amphibolite facies metamorphism (Li, 1979; Li, 1982; Li, Zhi, Chen, Wang, & Deng, 1983).

Magnetite occurs widely in various rocks and can also occur as ore minerals in many types of deposits (Dupuis & Beaudoin, 2011). Magnetite is an important petrogenetic indicator and pathfinder mineral with a wide array of applications including geophysical studies, igneous petrology, provenance studies, and mineral exploration (Nadoll, Angerer, Mauk, French, & Walshe, 2014). Most of the previous studies employed electron microprobe analysis, which measures a limited number of trace elements such as Mg, Al, Ca, Ti, V, Cr, and Mn with a relatively high detection limit of ~0.01 wt.%. However, recent development of laser ablation inductively coupled plasma mass spectrometry (LA-ICP-MS) technique provides in situ measurement of abundant trace elements with detection limits as low as sub ppm (Liu, Zhou, Chen, Gao, & Huang, 2015). Recent studies have demonstrated that chemical composition of magnetite by LA-ICP-MS thus can be used to fingerprint the types of mineral deposits and to distinguish different ore forming processes (Dare, Barnes, & Beaudoin, 2012; Huang, Gao, Qi, & Zhou, 2015; Li & Li, 2016; Nadoll, Mauk, Hayes, Koenig, & Box, 2012; Nadoll et al., 2014; Zhou, Tang, Chen, & Chen, 2017).

Valid geothermobarometry is a fundamentally important tool in deciphering the metamorphic conditions, and the garnet–biotite (GB) geothermometry is widely used in metapelitic rocks (Wu & Cheng, 2006). The BIFs in China experienced intense metamorphism and deformation and are therefore termed as sedimentary metamorphic-type iron deposits (Li et al., 2014). The staurolite-garnet-biotite schist, which is the wall-rock of the Gongchangling high-grade iron ore, is suitable to estimate the metamorphic temperature by GB geothermometry.

Magnetite is the main ore mineral of Gongchangling iron deposit. Therefore, in this paper, we present the in situ LA-ICP-MS data of magnetite of the Gongchangling iron deposit, and the mineral chemistry of garnet and biotite from the wall-rock for GB geothermometry were also obtained to constrain the genesis of high-grade iron ore.

2 | GEOLOGICAL BACKGROUND

2.1 | Regional geology

The NCC is one of the oldest cratonic blocks in the world, preserving rocks as old as ~3.85 Ga in the Anshan area of Liaoning Province (Song, Nutman, Liu, & Wu, 1996). The NCC consists of Archean to Paleoproterozoic basement overlain by Mesoproterozoic to Cenozoic cover (Zhao & Zhai, 2013). Zhai and Santosh (2011) proposed that the Precambrian crustal growth and stabilization of the NCC involved three main phases: (a) a major phase of continental growth at ~2.7 Ga; (b) the amalgamation of microblocks and cratonization at ~2.5 Ga; and (c) Paleoproterozoic rifting–subduction–accretion–collision tectonics and subsequent high-grade granulite facies metamorphism–granitoid magmatism during ~2.0–1.82 Ga. Based on the lithological assemblages, structural evidences, geochemical and geochronological data, and metamorphic P–T paths of Precambrian metamorphic rocks, the basement of the NCC has been subdivided into the Western Block (WB), the Eastern Block (EB), and the Trans–North China Orogen. It is proposed that the WB was formed by the amalgamation of the Yinshan Block in the north and the Ordos Block in the south along the E–W trending Khondalite Belt at ~1.95 Ga; the EB underwent a Paleoproterozoic rifting at 1.9–2.1 Ga with formation of the Jiao-Liao-Ji Belt; and collision of the WB and EB at ~1.85 Ga along the N-S-trending Trans–North China Orogen resulted in the final amalgamation of the NCC (Li, Zhao, & Sun, 2016; Li, Li et al., 2015a; Zhao, Sun, Wilde, & Li, 2005).

The Anshan-Benxi area located in the north part of the EB is characterized by a long geological history from 3.8 to 2.5 Ga and wide distribution of BIFs, containing the early Precambrian Anshan Group and Liaohe Group (Figure 1; Wan et al., 2012). In this area, an unconformity separates the underlying Archean Anshan Group from the overlying early Paleoproterozoic Liaohe Group, and both the Anshan and Liaohe groups are overlain unconformably by undeformed late Proterozoic sediments (Chen & Zhao, 1997; Li, Yang et al., 2015b; Tang, Chen, Santosh, Zhong, & Yang, 2013b; Tang, Chen, Santosh, Zhong, Wu & Lai, 2013a; Zhai, Sills, & Windley, 1990a; Zhai & Windley, 1990; Zhai, Windley, & Sills, 1990b).

The Anshan basement is subdivided into three parts: Tiejiashan gneisses, Anshan gneisses, and Anshan supracrustal rocks (namely, the Anshan Group). The Tiejiashan gneisses, which determined zircon U–Pb age of 2962 ± 4 and 2964 ± 6 Ma, with an area of over 25 km^2, form the basement of the Anshan Group. The Anshan gneisses, which yielded zircon U–Pb age of 2474 ± 13 Ma, intruded into the Anshan Group, resulting in the Anshan Group being observed as variable-sized enclaves in the gneisses (Song et al., 1996). The main rock types of the Anshan Group consist of amphibolite, leptynite, schist, migmatite, BIFs, siliceous rock, and carbonate on the whole. The Anshan Group is subdivided into the lower, middle, and upper Anshan Group, and the BIFs in this area mainly occur in the middle and upper Anshan Group (Zhou, 1994). Recent zircon U–Pb studies indicate that the BIFs in the Anshan-Benxi area were mainly formed at the late Neoarchean ages (2.55–2.50 Ga), except for the Dagushan iron ore deposit, which was dated at Mesoarchean (Dai et al., 2014; Wan et al., 2012).

2.2 | Deposit geology

The Gongchangling iron deposit is situated in the Anshan-Benxi area, Liaoning Province, and occurs as enclaves within large area of migmatite. The Gongchangling iron deposit comprises four mining areas: the No.1–3 mining areas and Laoling-Bapanling mining area (Chi, 1993). The Gongchangling No.2 mining area, the main high-grade iron ore distribution area, is located in the north limb of the Gongchangling anticline (Chi, 1993; Zhou, 1994). It is bounded by

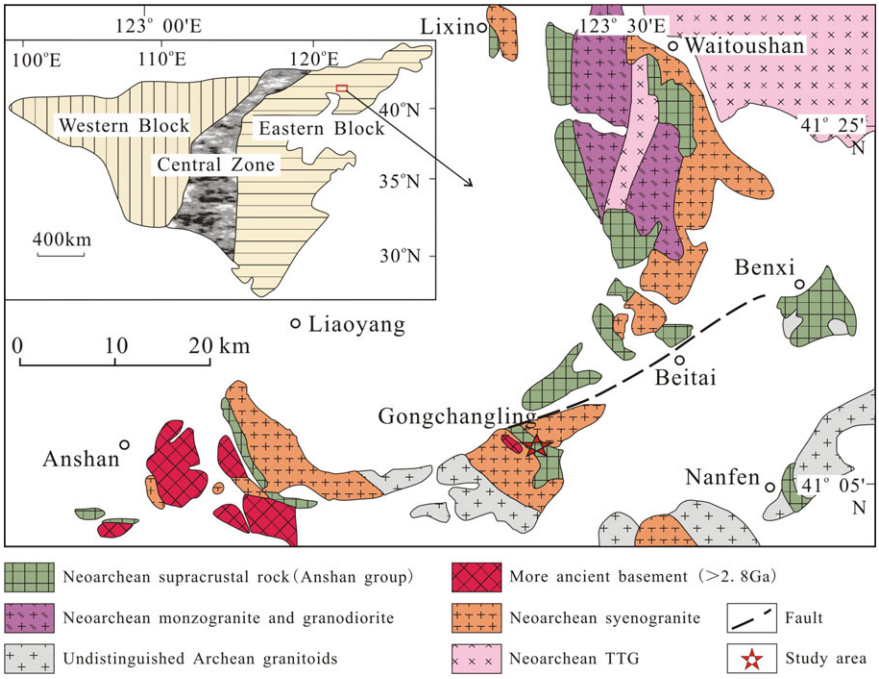

FIGURE 1 Geological map of the Anshan-Benxi, Liaoning Province (modified after Wan, 1993; Zhou, 1994)

the Hanling and Pianling faults in the northwest and southeast, respectively (Figure 2). The strata units of the Gongchangling No.2 mining area are briefly given as follows from bottom to top: (a) lower amphibolite; (b) lower schist; (c) lower iron ore belt: composed of Fe1 (Fe1-Fe6 means the first to the sixth layer of BIFs), middle schist, and Fe2; (d) middle leptynite: interlayer with Fe3; (e) upper iron ore belt: composed of Fe4, lower amphibolite, Fe5, upper amphibolites, and Fe6; and (f) Siliceous rock (Figure 3). The zircon SHRIMP U–Pb dating of leptynites, which were an interlayer of BIFs in the Gongchangling No.2 mining area, indicates that the BIFs were formed at late Neoarchean (2528 ± 10 Ma; Wan et al., 2012).

The Gongchangling No.2 mining area consists of six layers of BIFs. The ore layers are about 4,500 m in length, 300–600 m in width, and more than 1,000 m in depth and are hosted by the metamorphic rock series of the Cigou Formation of the Anshan Group (Wan, 1993). The ore layers that are narrowly strip-shaped strike SE with the angle of 120–160° and dip NE with dip angle of 60–80°, which is consistent with the occurrence of the wall-rocks. The iron ores are characterized by banded (BIFs) or massive (high-grade iron ore) structure and granular texture, and the four types of iron ore are recognized as follows: low-grade magnetite ore, high-grade magnetite ore, low-grade martite ore, and high-grade martite ore; nevertheless, magnetite ore is the major type (Chi, 1993).

The high-grade iron ore shows stratiform or stratiform-like occurrence, which is consistent with BIFs, and it mainly occurred within the ore layer of Fe6, accounting for 77.1% of the total high-grade ore reserves in the Gongchangling No.2 mining area (Li, Yang et al., 2015b). Strike reverse faults and transverse faults are well developed in this area, and the strike reverse faults developed during regional metamorphism period along the ore layer of Fe6, whereas the transverse faults developed after mineralization period (Zhou, 1994). The wall-rocks of high-grade iron ores exhibit obvious alteration zoning in sequence of cummingtonitization, garnetization, and chloritization outwards from the ore bodies, successively (Zhao & Li, 1980; Zhou, 1994).

3 | SAMPLING AND PETROGRAPHY

The BIFs in the Gongchangling No.2 mining area show banded structure, alternating the presence of black band (magnetite-rich) and white

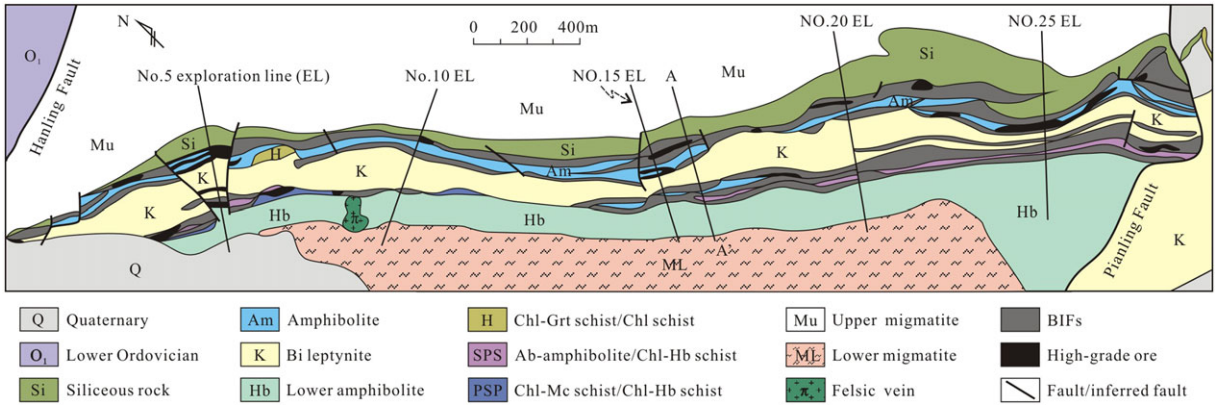

FIGURE 2 Geological map of the Gongchangling No.2 mining area (modified after Zhou, 1994)

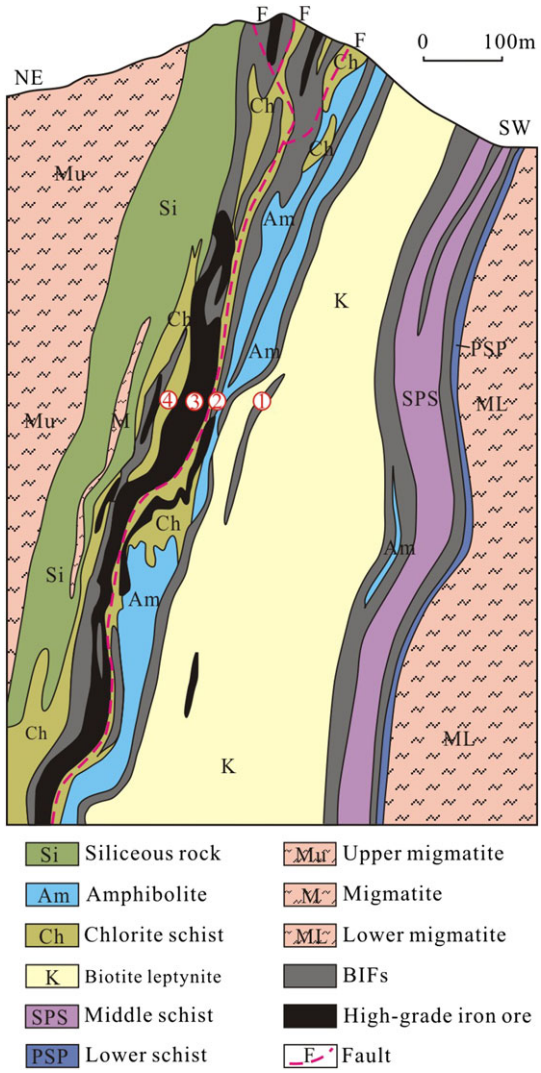

FIGURE 3 Cross section (A-A′in Figure 2) of the Gongchangling No.2 mining area (modified after Chi, 1993; Zhou, 1994). Sample locations: ①, act-bearing BIFs; ②, BIFs; ③, high-grade iron ore; ④, staurolite-garnet-biotite schist

band (quartz-rich). The black bands are essentially composed of magnetite and less abundant microcrystalline quartz, whereas the white bands mainly consist of quartz, minor actinolite, and magnetite. The BIFs are usually low-grade iron ores (20% < TFe < 45%), whereas the high-grade iron ore (TFe ≥ 45%) is a massive structure and mainly consists of magnetite (Sun et al., 2014; Zhou, 1994).

Three types of iron ore samples including BIFs without actinolite, actinolite-bearing BIFs, and high-grade iron ore were collected from the Gongchangling No.2 mining area, mining tunnel with a depth of 280 m. Magnetite from these different modes of occurrence was selected for trace elemental analysis. Staurolite-garnet-biotite schist is the wall-rock of high-grade iron ore; the composition of garnet and biotite were analysed by electron probe micro-analyzer (EPMA), and the garnet-biotite geothermometry is used to evaluate the metamorphism.

3.1 | Magnetite

Magnetite is the main ore mineral of the Gongchangling iron ore deposit. Magnetite in BIFs with/without actinolite occurs as anhedral to subhedral grains ranging from 0.02 to 0.3 mm in size (Figure 4a,b). Magnetite in high-grade iron ore is euhedral to subhedral grains with the size varying from 0.1 to 0.8 mm (Figure 4c,d).

3.2 | Garnet

Garnet is a common mineral in the Gongchangling No.2 mining area; it is mainly distributed in the altered wall-rocks, and it is more widely distributed in the upper iron ore belt than in the lower belt (Zhou, 1994). The garnet of this study is from staurolite-garnet-biotite schist, which is the wall-rock of high-grade iron ore of upper iron ore belt. The analysed euhedral garnet developed fissures and contains quartz inclusions, forming diablastic texture (Figure 4e, f).

3.3 | Biotite

Biotite is widely distributed in the study area, especially at the deep part. The biotite, which coexists with the garnet from staurolite-garnet-biotite schist, is subhedral to anhedral and exhibits obvious pleochroism, occurring as tabular crystals (Figure 4e,f).

4 | ANALYTICAL METHODS

4.1 | LA-ICP-MS

Trace elements of magnetite were performed by a Coherent GeoLasPro 193-nm Laser Ablation system coupled with an Agilent 7700× ICP-MS at the State Key Laboratory of Ore Deposit Geochemistry, Institute of Geochemistry, Chinese Academy of Sciences, Guiyang, China. Analytical methods are available in Huang, Zhou, Qi, Gao, and Wang (2013). Helium, as a carrier gas, and argon, as a makeup gas, were mixed via a T-connector prior to the entering of the ICP. One hundred and sixty successive laser pulses (4 Hz) in a size of 44 μm ablated the surfaces of the sample for about 40 s after monitoring the gas blank for 20 s for each analysis. Element contents were calibrated against multiple reference materials (GSE-1G, BCR-2G, BIR-1G, BHVO-2G, and NIST610) using ^{57}Fe as the internal standard (Liu et al., 2008). Every eight sample analyses were followed by one analysis of GSE-1G as quality control to correct the time-dependent drift of sensitivity and mass discrimination. Offline selection and integration of background and analytic signals and time drift correction and quantitative calibration were performed by ICPMSDataCal (Liu et al., 2008). Detailed operating conditions for the laser ablation system and the ICP-MS instrument and data reduction are described in Liu et al. (2008).

4.2 | EPMA

Mineral chemical composition of garnet and biotite was determined by wavelength-dispersive X-ray emission spectrometry using an EPMA-1600 electron microprobe at the Institute of Geochemistry, Chinese Academy of Sciences in Guiyang, China. The analytical conditions were as follows: beam current of 10 nA, acceleration voltage of 25 kV, and a beam size of 10 μm in diameter. The detection limit for these elements under such conditions is 0.01%, and the analytical reproducibility is

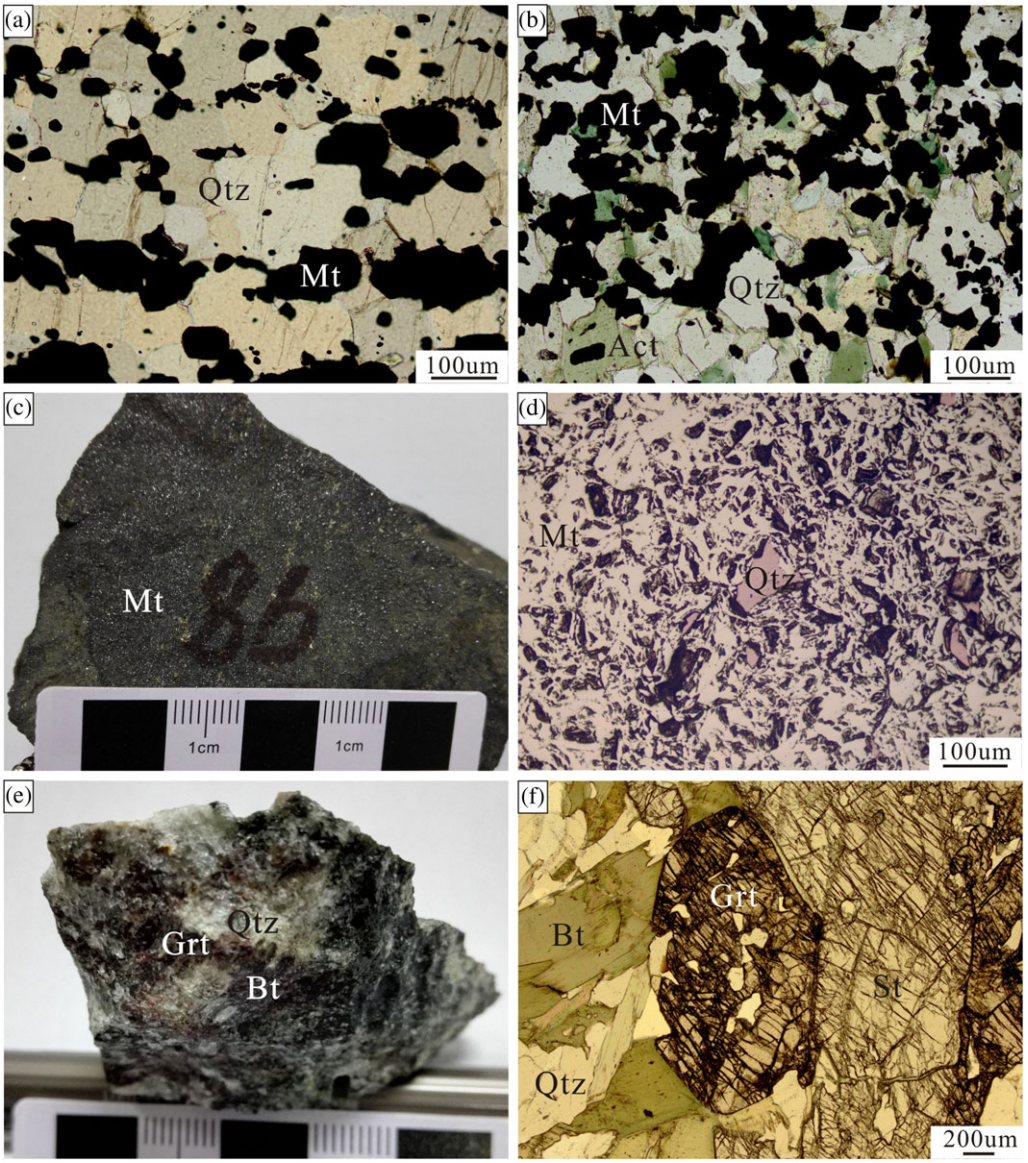

FIGURE 4 Photos and photomicrographs of different occurrence modes of magnetite and associated wall-rocks from the Gongchangling No. 2 mining area. (a) BIFs, banded structure and mainly composed of magnetite and quartz, under transmitted light; (b) actinolite-bearing BIFs, consisting of magnetite, quartz and actinolite, under transmitted light; (c) high-grade iron ore with massive structure; (d) high-grade iron ore, magnetite coexisting with minor quartz, under reflected-light; (e) schist, wall-rock of high-grade iron ore; (f) Staurolite-garnet-biotite schist, mainly consisting of staurolite, garnet, biotite, and quartz, and the garnet containing quartz inclusions, forming diablastic texture, under transmitted light. Mt = magnetite; Qtz = quartz; Act = actinolite; St = staurolite; Grt = garnet; Bt = biotite

within 2%. The counting time was 20–40 s for major elements and 40–60 s for minor elements. SPI mineral standards (USA) were used for calibration.

5 | ANALYTICAL RESULTS

5.1 | In situ LA-ICP-MS analysis

The magnetite is selected from three modes of occurrence: BIFs (without actinolite), actinolite-bearing BIFs, and high-grade iron ore. According to Dare et al. (2012), trace elements in magnetite can be lithophile elements (Mg, Al, Cr, Ga, Mn, Nb, Ta, Ti, V, Zr, and Hf) and chalcophile elements (Co, Mo, Ni, Pb, Sn, and Zn). However, only a suite of elements, namely, Mg, Al, Ti, V, Co, Ni, Zn, Cr, Mn, Ga, and Sn, are commonly present in magnetite of all origins and can be used as main discriminator elements for magnetite (Nadoll et al., 2014). The average trace elemental compositions of magnetite are presented in Table 1, and the detailed analytical results are given in the e-Appendix 1. The magnetite grains from the Gongchangling No.2 mining area show that the contents of Mg, Al, V, Mn, Co, Ni, Zn, Cr, and Ga are all above the detection limits, whereas a few spots with Ti and Sn contents are below the detection limits. Other trace elements that were also analysed in magnetite by LA-ICP-MS include Sc, Cu, Ge, Rb, Sr, Y, Zr, Nb, Mo, Ag, Cd, In, Ba, Hf, Ta, W, Bi, Pb, Th, and U, but their contents are generally either below the detection limits or below 1 ppm. As showed in e-Appendix 1, trace element contents in magnetite of every mode of occurrence are concentrated and generally vary less than one order of magnitude. However, compositional variations between different modes of occurrence in magnetite can be further

TABLE 1 LA-ICP-MS results for trace elements (in ppm) of magnetite from the Gongchangling No.2 mining area

Sample no.		Mg	Al	Ti	V	Cr	Mn	Co	Ni	Zn	Ga	Sn
D.L.		4.01	2.83	3.66	0.13	1.96	1.44	0.10	1.50	0.64	0.09	0.40
10GCL-3	AVE (n = 12)	98.0	984	56.6	11.0	26.7	305	1.50	7.24	21.27	2.33	1.37
BIFs	SD	75.5	375	14.4	2.10	26.9	26.7	0.57	2.34	3.98	0.51	0.48
10GCL-14	AVE (n = 12)	34.1	532	413	35.9	36.9	44.8	2.00	3.42	4.41	3.30	0.42
Act-BIFs	SD	28.7	42	26	3.85	35.3	2.25	0.36	0.94	1.32	0.40	0.69
10GCL-86	AVE (n = 12)	72.5	1943	2.66	3.38	5.49	330	3.11	5.40	28.93	1.38	22.7
High-grade	SD	39.9	50	2.22	0.35	1.88	12.06	0.26	1.35	3.51	0.20	1.90

Note. Act = actinolite; AVE = average; BIFs = banded iron formations; D.L. = detection limit; LA-ICP-MS = laser ablation inductively coupled plasma mass spectrometry; n = number of analytical points; SD = standard deviation.

identified by normalized multielemental patterns (Figure 5) and binary plots of selected elements (Figure 6).

5.1.1 | Magnetite from BIFs without actinolite

Magnetite from the BIFs, which mainly consist of magnetite and quartz without actinolite, typically contains highest contents of Mg (average of 98 ppm) and moderate contents of Ti (average of 56.5 ppm), V (average of 11 ppm), and Al (average of 984 ppm). The contents of Ti and V of magnetite from BIFs are within it from actinolite-bearing BIFs and high-grade iron ore.

5.1.2 | Magnetite from actinolite-bearing BIFs

The trace elemental concentrations of magnetite from actinolite-bearing BIFs are relatively rich in Ti (average of 413 ppm) and V (average of 36 ppm), and these elements are distinctively higher than magnetite from BIFs without actinolite and high-grade iron ore. Moreover, the magnetite is relatively poorer in contents of Mg (average of 34.1 ppm), Al (average of 532 ppm), Mn (average of 44.8 ppm), and Zn (average of 4.41 ppm).

5.1.3 | Magnetite from high-grade iron ore

The magnetite from high-grade iron ore contains relatively high contents of Al (average of 1943 ppm) and Sn (average of 22.7 ppm). The magnetite from high-grade iron ore shows the lowest contents of Ti (average of 2.66 ppm) and V (average of 3.38 ppm) compared with magnetite from BIFs (coexisting with/without actinolite).

On the whole, the contents of Ti and V in magnetite decrease from actinolite-bearing BIFs, through BIFs, to high-grade iron ore,

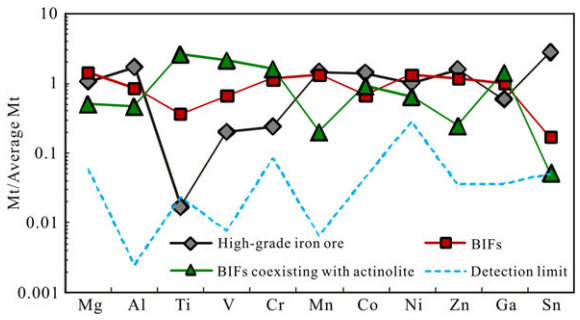

FIGURE 5 Normalized multi-elemental patterns of different occurrence modes of magnetite. Normalized values are the average composition of all the magnetite grains from the Gongchangling No.2 mining area

and Ti versus V grossly shows a positive correlation (Figure 6). In order to compare the composition variations between different types of magnetite, the trace element contents are normalized to the composition of all the magnetite grains from the Gongchangling No.2 mining area. Magnetite grains from the high-grade iron ore show distinguished patterns from the BIFs or actinolite-bearing BIFs, indicating the effect of hydrothermal alteration (Figure 5).

5.2 | EPMA analysis

The chemical compositions of garnet and biotite are listed in Table 2.

5.2.1 | Garnet

The EPMA surface scanning shows that the garnet is homogeneous in chemical composition without zoning (Figure 7). Chemically, the garnet is dominated by almandine (89.6–92.0%) and pyrope (7.7–10.0%), with minor spessartite (0–0.1%) and andradite (0–0.1%).

5.2.2 | Biotite

According to the iron-bearing coefficient ($f = Fe/(Fe + Mg) \times 100$), the biotite in the Gongchangling No.2 mining area can be divided into iron-poor (f = 20–50), iron-normal (f = 50–60), and iron-rich (f = 60–80) types (Zhou, 1994). High-grade iron ore has a close relationship with iron-rich biotite; and the iron-bearing coefficient of biotite may be used as a mark of searching for high-grade iron ore bodies in the Anshan-Benxi area (Zhou, 1994). The f values of the biotite in this study range from 63 to 68, with the average of 65, which is consistent with their occurrence of the wall-rock of high-grade iron ore.

6 | DISCUSSION

6.1 | Nature of different types of magnetite

Magnetite from the Gongchangling No.2 mining area exhibits compositional variations, which may reflect distinct origins of different types of magnetite. The compositional variations of magnetite from BIFs (without actinolite) and actinolite-bearing BIFs are mainly thought to reflect influence of coexisting minerals, whereas the compositional variations of magnetite from BIFs (coexisting with/without actinolite) and high-grade iron ore are believed to reflect modification of later hydrothermal fluids (Figure 5).

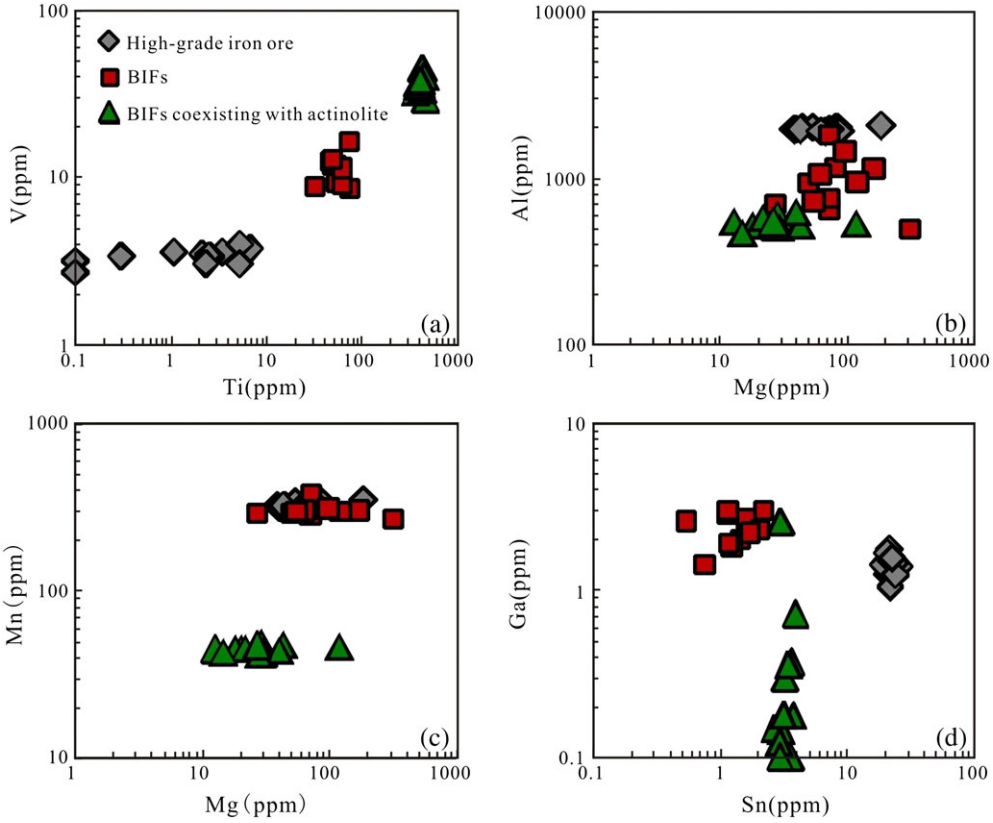

FIGURE 6 Bimodal plots of Ti versus V (a), Mg versus Al (b), Mg versus Mn (c), and Sn versus Ga (d) of magnetite from the Gongchangling No.2 mining area

6.1.1 | Influence of coexisting mineral on the magnetite composition from BIFs

Coexisting mineral phases, such as silicate and sulphide, generally play significant roles on the trace elemental composition of magnetite due to later reaction between magnetite and these minerals (Chung, Zhou, Gao, & Chen, 2015; Nadoll et al., 2014).

In general, silicates are preferably incorporating lithophile elements, whereas chalcophile elements have a strong preference to partition into sulfides. Because V, Cr, and Ti are not easily incorporated into the actinolite compared to magnetite in BIFs, it rarely affected their concentrations in magnetite. For the presence of V, Cr, and Ti in seawater, composition is prone to the effect of hydrothermal fluid related to mafic–ultramafic rocks (Bhattacharya, Chakrabortym, & Ghosh, 2007), and the geochemical study of Gongchangling iron ore indicated that the mixture of seawater and hydrothermal fluid that percolated and dissolved the submarine volcanic rocks provided the ore-forming material (Sun et al., 2014). Thus, the higher contents of V, Cr, and Ti in magnetite from actinolite-bearing BIFs compared to the magnetite without coexisting actinolite may reflect that the formation of actinolite-bearing BIFs suffered more intense hydrothermal fluid. Mg, Al, Mn, and Zn can replace corresponding ions in actinolite as the mode of isomorphism, so the magnetite from BIFs coexisting with actinolite shows relatively low contents of Mg, Al, Mn, and Zn (Figure 6).

6.1.2 | Magnetite from high-grade iron ore as modification by later hydrothermal fluid

Vanadium has a range of possible valence states in natural fluid (including V^{3+}, V^{4+}, and V^{5+}), but only V^{3+} is usually preferentially incorporated into the magnetite structure at low oxygen fugacity, and V becomes incompatible at high oxygen fugacity due to its 5+ oxidation state. Therefore, V content in magnetite may be controlled by fO_2, and vanadium is preferably enriched in relatively reduced fluids (Chung et al., 2015; Nadoll et al., 2014; Zhou et al., 2017). The magnetite from high-grade iron ore has extremely low V concentration compared to its counterpart from BIFs (with/without actinolite), indicating that the high-grade iron ore may be reformed by the relatively oxidized hydrothermal fluid.

Aluminium is preferably linked with high temperature such as in a magmatic system and considered to be immobile at submagmatic temperatures, and its incorporation in magnetite is largely temperature controlled (Verlaguet, Brunet, Goffé, & Murphy, 2006). The enrichment of Al in high-grade iron ore suggests a relatively high temperature alteration. The Ti + V versus Al + Mn plot displays clear positive correlation between temperature and Ti + V, Al + Mn contents (Nadoll et al., 2014; Zhou et al., 2017). In the (Al + Mn) versus (Ti + V) diagram (Figure 8), the magnetite samples from BIFs (coexisting with/without actinolite) are plotted in the field of 200–300 °C, whereas magnetite grains from high-grade iron ore are plotted nearby the field for the lower contents of Ti and V. The obviously positive Eu anomalies of the Gongchangling BIFs and high-grade iron ores suggest that high temperature hydrothermal fluid (> 250 °C) is associated with the formation of the Gongchangling iron ore deposit (Sun et al., 2014). Temperature recorded for hydrothermal alteration is approximately 100 to 300 °C for BIF-hosted high-grade ore (Thorne, Hagemann, Webb, & Clout, 2008). Therefore, it is inferred that the high temperature hydrothermal fluid (ca. 250–300 °C) may be involved in the formation of the

TABLE 2 Representative composition of garnet and biotite from the Gongchangling No.2 mining area

Garnet	Grt-01	Grt-02	Grt-03	Grt-04	Grt-05	Grt-06	Grt-07	Grt-08	Grt-09	Grt-10	Grt-11	Grt-12	Grt-13	Grt-14	Grt-15	Grt-16	Grt-17
SiO_2	36.12	35.30	35.13	36.11	35.86	36.24	36.30	35.99	36.48	35.39	36.60	36.46	36.40	35.49	35.88	36.19	34.84
TiO_2	0.02	0.04	0.00	0.02	0.03	0.01	0.04	0.02	0.06	0.05	0.04	0.04	0.00	0.01	0.01	0.02	0.01
Al_2O_3	20.46	20.83	20.55	20.77	20.74	20.47	20.50	20.75	20.90	20.43	20.67	20.44	20.34	20.84	20.49	20.75	20.02
Cr_2O_3	0.01	0.00	0.02	0.00	0.00	0.02	0.01	0.00	0.01	0.00	0.02	0.00	0.00	0.00	0.01	0.00	0.00
FeO	40.37	40.55	41.00	40.99	40.96	40.83	41.01	41.16	41.19	41.08	40.80	40.85	40.60	41.43	40.79	41.31	40.86
MnO	0.01	0.04	0.02	0.02	0.04	0.00	0.03	0.00	0.03	0.04	0.03	0.04	0.03	0.03	0.02	0.01	0.00
MgO	2.24	2.27	2.35	2.15	2.27	2.08	2.10	2.15	2.11	2.24	1.90	2.30	2.28	1.83	2.23	2.23	2.20
CaO	0.15	0.10	0.11	0.11	0.08	0.10	0.09	0.08	0.09	0.09	0.08	0.10	0.09	0.07	0.09	0.12	0.08
Na_2O	0.00	0.00	0.02	0.00	0.00	0.00	0.00	0.00	0.00	0.00	0.00	0.00	0.00	0.00	0.00	0.01	0.00
K_2O	0.00	0.00	0.00	0.00	0.02	0.00	0.01	0.00	0.00	0.00	0.01	0.00	0.01	0.01	0.00	0.00	0.01
Total	99.38	99.12	99.20	100.17	99.99	99.75	100.08	100.15	100.87	99.34	100.14	100.21	99.75	99.71	99.52	100.64	98.03
Si	2.963	2.902	2.887	2.941	2.924	2.966	2.961	2.933	2.951	2.909	2.985	2.967	2.975	2.910	2.941	2.933	2.903
Ti	0.001	0.002	0.000	0.001	0.002	0.001	0.002	0.001	0.004	0.003	0.002	0.002	0.000	0.001	0.001	0.001	0.001
Al	1.978	2.019	1.991	1.994	1.994	1.975	1.972	1.993	1.993	1.980	1.987	1.961	1.960	2.015	1.980	1.983	1.967
Cr	0.001	0.000	0.001	0.000	0.000	0.001	0.001	0.000	0.001	0.000	0.001	0.000	0.000	0.000	0.001	0.000	0.000
Fe^{3+}	0.093	0.173	0.236	0.122	0.157	0.091	0.102	0.139	0.096	0.197	0.038	0.101	0.090	0.164	0.136	0.149	0.226
Fe^{2+}	2.676	2.614	2.582	2.670	2.636	2.704	2.696	2.666	2.691	2.627	2.745	2.679	2.686	2.677	2.660	2.651	2.621
Mn	0.001	0.003	0.001	0.001	0.003	0.000	0.002	0.000	0.002	0.003	0.002	0.003	0.002	0.002	0.001	0.001	0.000
Mg	0.274	0.278	0.288	0.261	0.276	0.254	0.255	0.261	0.254	0.274	0.231	0.279	0.278	0.224	0.272	0.269	0.273
Ca	0.013	0.009	0.010	0.010	0.007	0.009	0.008	0.007	0.008	0.008	0.007	0.009	0.008	0.006	0.008	0.010	0.007
Na	0.000	0.000	0.003	0.000	0.000	0.000	0.000	0.000	0.000	0.000	0.000	0.000	0.000	0.000	0.000	0.002	0.000
K	0.000	0.000	0.000	0.000	0.002	0.000	0.001	0.000	0.000	0.000	0.001	0.000	0.001	0.001	0.000	0.000	0.001
Sum	8.000	8.000	7.999	8.000	8.001	8.001	8.000	8.000	8.000	8.001	7.999	8.001	8.000	8.000	8.000	7.999	7.999
Biotite	Bt-01	Bt-02	Bt-03	Bt-04	Bt-05	Bt-06	Bt-07	Bt-08	Bt-09	Bt-10	Bt-11	Bt-12	Bt-13	Bt-14	Bt-15	Bt-16	Bt-17
SiO_2	34.67	35.42	35.90	34.36	35.57	34.83	35.41	35.77	33.93	34.42	34.95	35.06	34.94	36.03	35.06	35.08	34.59
TiO_2	0.27	0.22	0.23	0.19	0.27	0.16	0.25	0.17	0.16	0.16	0.10	0.15	0.13	0.16	0.16	0.14	0.13
Al_2O_3	20.48	20.22	19.98	20.06	20.07	20.33	20.46	20.48	19.77	20.07	20.46	20.02	20.46	20.73	20.13	20.51	20.36
FeO	24.55	23.80	25.04	26.53	24.38	24.28	23.62	23.31	25.35	24.61	24.59	23.90	23.90	22.52	24.45	23.97	25.65
MnO	0.00	0.00	0.01	0.03	0.00	0.00	0.01	0.00	0.00	0.01	0.00	0.01	0.00	0.00	0.00	0.00	0.00
MgO	6.85	7.47	7.03	7.09	7.17	7.18	7.21	7.52	7.44	7.43	6.99	7.21	7.21	7.56	7.26	7.31	6.99
CaO	0.00	0.00	0.00	0.00	0.00	0.00	0.00	0.00	0.00	0.00	0.00	0.00	0.00	0.00	0.00	0.00	0.00
Na_2O	0.04	0.03	0.03	0.02	0.04	0.01	0.01	0.03	0.02	0.03	0.02	0.03	0.00	0.04	0.02	0.03	0.02
K_2O	8.41	8.25	8.40	7.29	8.36	8.57	8.50	8.52	7.26	7.76	7.42	8.50	8.53	8.65	8.45	8.47	7.31
Total	95.27	95.40	96.62	95.57	95.86	95.37	95.47	95.81	93.94	94.50	94.53	94.87	95.16	95.69	95.54	95.50	95.05
Si	2.665	2.702	2.721	2.632	2.711	2.672	2.708	2.720	2.636	2.652	2.679	2.702	2.682	2.740	2.683	2.681	2.651

(Continues)

TABLE 2 (Continued)

Garnet	Grt-01	Grt-02	Grt-03	Grt-04	Grt-05	Grt-06	Grt-07	Grt-08	Grt-09	Grt-10	Grt-11	Grt-12	Grt-13	Grt-14	Grt-15	Grt-16	Grt-17
Al^{total}	1.856	1.818	1.785	1.812	1.804	1.839	1.845	1.835	1.811	1.823	1.849	1.819	1.851	1.859	1.816	1.847	1.840
^{IV}Al	1.335	1.298	1.279	1.368	1.289	1.328	1.292	1.280	1.364	1.348	1.321	1.298	1.318	1.260	1.317	1.319	1.349
^{VI}Al	0.521	0.520	0.506	0.444	0.515	0.511	0.553	0.555	0.447	0.475	0.528	0.521	0.533	0.599	0.499	0.528	0.491
Fe^{2+}	1.427	1.373	1.456	1.445	1.431	1.400	1.431	1.409	1.400	1.348	1.340	1.422	1.400	1.433	1.393	1.386	1.397
Mg	0.785	0.849	0.793	0.809	0.815	0.821	0.822	0.852	0.862	0.853	0.799	0.829	0.825	0.857	0.827	0.832	0.798
Ti	0.015	0.012	0.013	0.011	0.015	0.009	0.014	0.010	0.010	0.009	0.006	0.009	0.007	0.009	0.009	0.008	0.008
Cr	0.000	0.000	0.000	0.000	0.000	0.000	0.000	0.000	0.000	0.000	0.000	0.000	0.000	0.000	0.000	0.000	0.000
Fe^{3+}	0.152	0.146	0.131	0.255	0.123	0.158	0.080	0.074	0.247	0.238	0.236	0.118	0.135	0.000	0.172	0.145	0.247
Mn	0.000	0.000	0.001	0.002	0.000	0.000	0.001	0.000	0.000	0.001	0.000	0.000	0.000	0.000	0.000	0.000	0.000
Ca	0.000	0.000	0.000	0.000	0.000	0.000	0.000	0.000	0.000	0.000	0.000	0.000	0.000	0.000	0.000	0.000	0.000
Na	0.007	0.005	0.004	0.003	0.006	0.001	0.002	0.005	0.003	0.004	0.003	0.005	0.000	0.005	0.004	0.004	0.003
K	0.824	0.803	0.812	0.712	0.813	0.839	0.829	0.827	0.720	0.763	0.725	0.836	0.835	0.839	0.825	0.826	0.715
Sum	7.732	7.709	7.717	7.682	7.720	7.741	7.732	7.733	7.688	7.692	7.637	7.741	7.736	7.744	7.729	7.731	7.658
T (°C)	611	597	630	598	608	583	588	586	574	588	562	603	600	562	596	594	607

Note. The amount of Fe^{3+} was calculated from stoichiometric constraints using program AXE (Powell, Holland, & Worley, 1998). The temperature (T) was calculated based on the garnet-biotite thermometry proposed by Holdaway (2000).

Gongchangling BIFs, and this is in accordance with the geochemical study, which indicated that ore-forming material of the Gongchangling BIFs is from the mixture of seawater and hydrothermal fluid (Sun et al., 2014). The high-grade iron ore may be reformed by later high-temperature and relatively oxidized fluid resulting in the lower contents of Ti and V (Figure 8).

In summary, based on the compositional variation of magnetite from BIFs and high-grade iron ore, it indicates that the magnetite from high-grade iron ore may be reformed by high temperature and relatively oxidized fluid.

6.2 | Metamorphism of the wall-rock of high-grade iron ore

It is generally considered that the Anshan Group supracrustal rocks in the Anshan-Benxi area suffered a varying degree of metamorphism from the west to the east, which varies from greenschist facies in Anshan, through amphibolite facies with diagnostic mineral of staurolite and kyanite in Liaoyang, to diagnostic mineral of sillimanite in Benxi (Zhou, 1994). However, Zhai, Sills, and Windley (1990a) proposed that the Anshan Group supracrustal rocks in Anshan-Benxi area all suffered amphibolite facies metamorphism, and the metamorphism increases from the west to the east, whereas retrograde metamorphism decreases from the west to the east (Zhai & Windley, 1990; Zhai, Sills, & Windley, 1990a; Zhai, Windley, & Sills, 1990b).

The mineral assemblage of garnet-biotite is common in magmatic rocks, especially in metamorphic rocks, and the Fe-Mg exchange of the two minerals has a functional relationship with equilibrium temperature, which can be used to calibrate garnet-biotite geothermometry (Holdaway, 2000; Wu, Zhang, & Ren, 2004). The pressure has limited effect on the geothermometry. It is estimated that the pressure of the study area is ~4–7 kbar (Zhai, Sills, & Windley, 1990a). Therefore, we set the pressure of 5 kbar and applied the garnet-biotite geothermometry to staurolite-garnet-biotite schist in order to calculate metamorphic temperature. It showed a relatively clustering result in the range of 562–630 °C, with a mean temperature of 593 °C and standard deviation 17 °C for 17 pairs, which are in agreement with the temperature estimated by hornblende-plagioclase geothermometry of amphibolites within the deviation range (Sun et al., 2014).

6.3 | Genesis of high-grade iron ore

The Gongchangling No.2 mining area outputs the main high-grade iron ore in the Anshan-Benxi area. However, the genesis of the high-grade iron ore in this area has been hotly debated for a long time, and more and more studies support the viewpoint that the high-grade iron ore is the hydrothermal fluid reformed BIFs; nevertheless, the hydrothermal nature is still in the debate between migmatitic hydrothermal fluid from magma (Chen et al., 1985; Cheng, 1957; Li et al., 1977; Li et al., 2012; Zhao & Li, 1980; Zhao et al., 1979) and metamorphic hydrothermal fluid from regional metamorphism (Guan, 1961; Shi & Li, 1980; Sun et al., 2014; Zhou, 1994).

In the discriminant diagrams, which were introduced by Dupuis and Beaudoin (2011) to identify different mineral deposit types

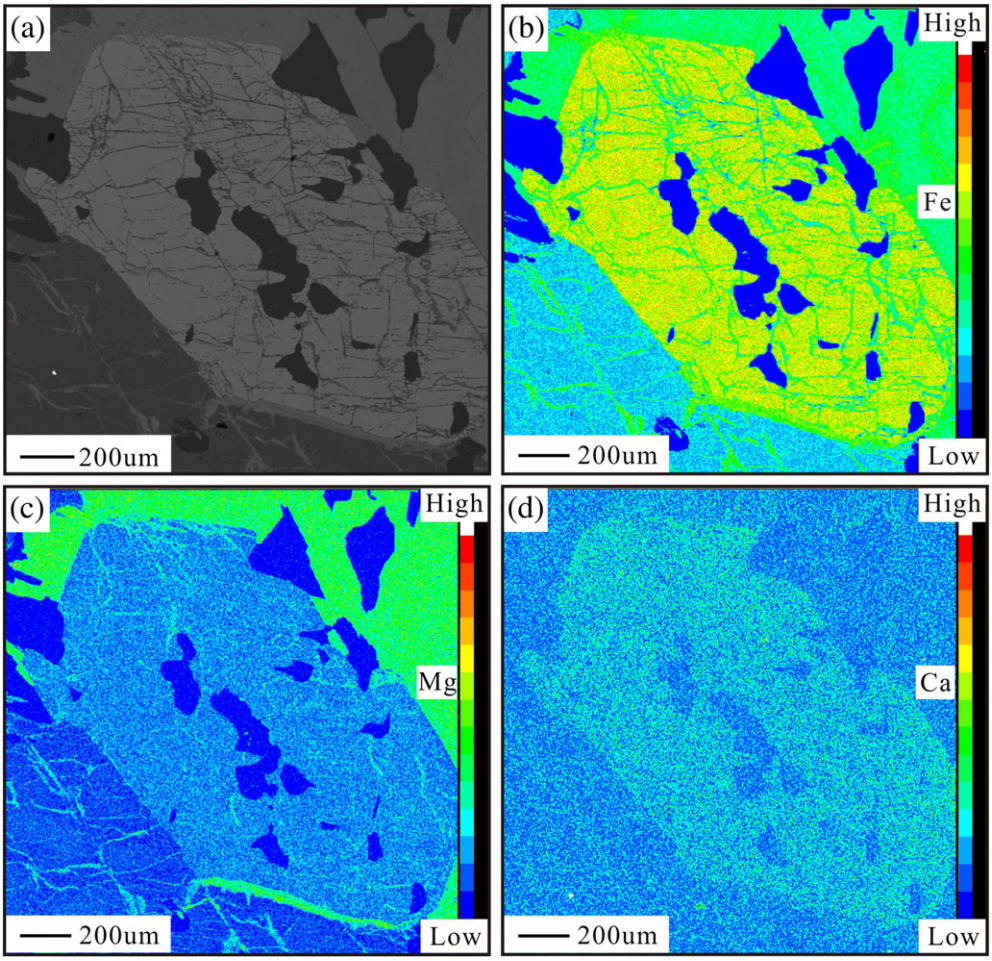

FIGURE 7 EPMA compositional map analysis of garnet from staurolite-garnet-biotite schist of the Gongchangling No.2 mining area. (a) BSE image; (b) Fe element; (c) Mg element; (d) Ca element

according to magnetite compositions (Figure 9), Nadoll et al. (2014) suggested that the "BIF" field would extend towards lower Ti + V, Ca + Al + Mn, and Ni/(Cr + Mn) values. Magnetite grains from BIFs (coexisting with/without silicate) are plotted in the "BIF" or "extended BIF" field, indicating the derivation of sedimentary process, whereas the magnetite samples from the high-grade iron ore are plotted in the "skarn" field, attributed to the later hydrothermal alternation.

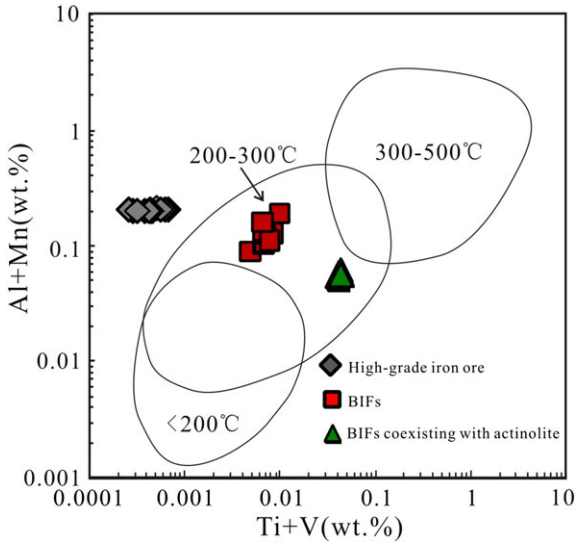

FIGURE 8 Plot of Al + Mn versus Ti + V for different formation temperature of magnetite. Reference fields are adapted from Nadoll et al. (2014) and Zhou et al. (2017)

With regard to the hydrothermal nature involved in the formation of high-grade iron ore, we prefer to hold that the formation of high-grade iron ore is related to the metamorphic hydrothermal fluid, considering that (a) the wall-rock alteration of high-grade iron ore is well developed in the Gongchangling No.2 mining area, and the intensity of wall-rock alteration is proportional to the scale of high-grade iron ore body in general (Zhou, 1994); (b) magnetite trace element compositions suggest that the magnetite from high-grade iron ore may be reformed by high temperature and relatively oxidized fluid, and it may be metamorphic hydrothermal fluid rather than migmatitic hydrothermal fluid. Because the metamorphic hydrothermal fluid is relatively oxidized compared with the migmatitic hydrothermal fluid in general (Liu, 1985), and the fluid inclusions of the high-grade iron ore have more SO_4^{2-} contents than counterpart of migmatite in the Gongchangling iron ore deposit (Li & Shi, 1979), indicating that the high-grade iron ore suffered more oxidized hydrothermal alteration than the migmatitic hydrothermal fluid; and (c) the staurolite-garnet-biotite, which is the wall-rock of high-grade iron ore, recorded the metamorphic temperature of 593 ± 17 °C, and the metamorphic hydrothermal

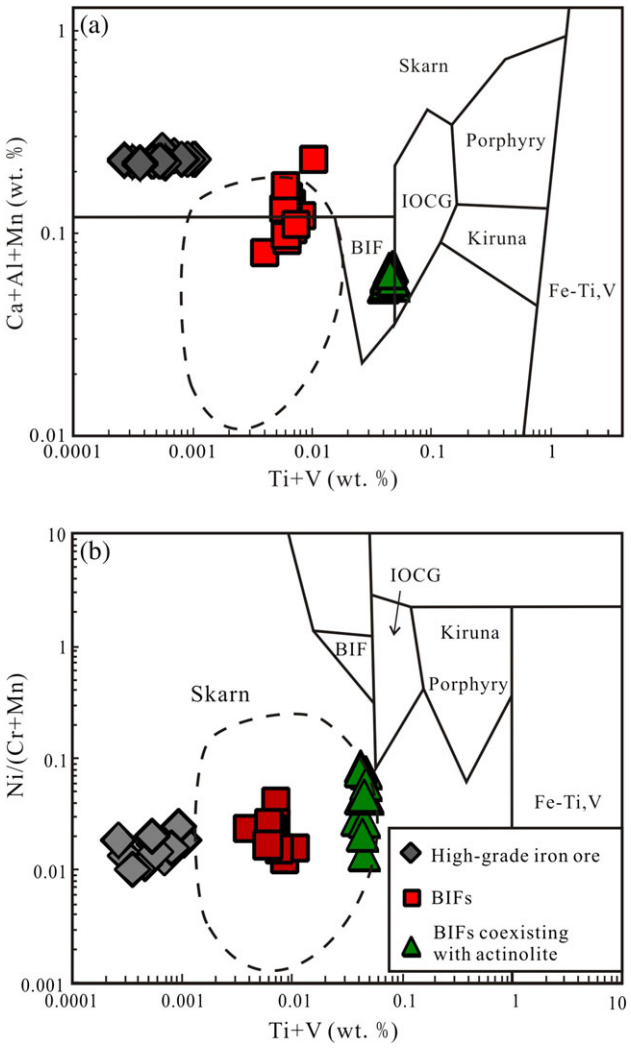

FIGURE 9 Plots of Ca + Al + Mn versus Ti + V (a) and Ni/(Cr + Mn) versus Ti + V (b) for LA-ICP-MS data of magnetite from the Gongchagnling No.2 mining area. Reference fields are adapted from Dupuis and Beaudoin (2011). BIF = banded iron formation; Skarn = Fe–Cu skarn deposits; IOCG = iron-oxide-copper-gold deposits; Porphyry = porphyry Cu deposits; Kiruna = Kiruna apatite-magnetite deposits; Fe–Ti, V = magmatic Fe–Ti-oxide deposits. Dashed line = "extended BIF field" according to Nadoll et al. (2014) and Chung et al. (2015)

fluid transferred along weak tectonic zone and reformed the BIFs to generate high-grade iron ore.

7 | CONCLUSIONS

1. Three types of magnetite from the Gongchangling No.2 mining area in Liaoning Province, NE China, exhibit different trace element composition. The compositional variations of magnetite from BIFs (without actinolite) and actinolite-bearing BIFs suggest that coexisting minerals have played an important role in the trace element concentration in magnetite, whereas the different compositions of magnetite from BIFs (coexisting with/without actinolite) and high-grade iron ore indicate that the high-grade iron ore may be reformed by high temperature and relatively oxidized hydrothermal fluid.
2. The staurolite-garnet-biotite schist, as the wall-rock of high-grade iron ore, recorded the metamorphic temperature of 593 ± 17 °C, which was estimated by the garnet-biotite geothermometry.
3. According to the trace element composition of magnetite and metamorphism of the wall-rock, combined with previous studies, it indicates that the genesis of high-grade iron ore may be related to the metamorphic hydrothermal alteration.

ACKNOWLEDGEMENTS

This work was financially supported by the National Natural Science Foundation of China (No. 41503035, 41672086), the Major State Basic Research Program of China (No. 2012CB416602), the Natural Science Basic Research Plan in Shaanxi Province of China (No. 2017JM4006, 2016JQ4010), and Fundamental Research Funds for the Central Universities (310827151060, 310827161007). We gratefully acknowledge Wen-Qin Zheng and Ting Zhou from the State Key Laboratory of Ore Deposit Geochemistry for their help in microprobe and LA-ICP-MS analysis. We are grateful to Prof. G.X. Yang and two anonymous reviewers for their careful corrections, relevant comments and constructive suggestions to the manuscript.

ORCID

Xiaohui Sun http://orcid.org/0000-0002-0018-8002
Yan Luan http://orcid.org/0000-0002-9430-4333

REFERENCES

Bekker, A., Slack, J. F., Planavsky, N., Krapež, B., Hofmann, A., Konhauser, K. O., & Rouxel, O. J. (2010). Iron formation: The sedimentary product of a complex interplay among mantle, tectonic, oceanic, and biospheric processes. *Economic Geology*, *105*, 467–508.

Bhattacharya, H. N., Chakrabortym, I., & Ghosh, K. K. (2007). Geochemistry of some banded iron-formations of the Archean Supracrustals, Jharkhand–Orissa region, India. *Journal of Earth System Science*, *116*, 245–259.

Chen, Y. J., & Zhao, Y. C. (1997). Geochemical characteristics and evolution of REE in the Early Precambrian sediments: Evidences from the southern margin of the North China Craton. *Episodes*, *20*, 109–116.

Chen, G. Y., Sun, D. S., Sun, C. M., Li, M. H., Wang, X. F., & Wang, Z. F. (1984). Genesis of Gongchangling iron deposit. *Journal of Mineralogy and Petrology*, *4*, 1–266. (in Chinese)

Chen, J. F., Yang, Y. L., Li, P., Cheng, W. J., Zhou, T. X., & Liu, Y. P. (1985). Sulfur isotope study on the genesis of high-grade iron deposit in Anshan-Benxi area, Liaoning Province. *Geology and Prospecting*, *21*, 32–37. (in Chinese)

Cheng, Y. Q. (1957). Problems on the high-grade ore in the Presinian (Precambrian) banded iron ore deposits of the Anshan type of Liaoning and Shandong Provinces. *Acta Geologica Sinica*, *33*, 153–180. (in Chinese with English abstract)

Chi, W. Z. (1993). Second mining area of the Gongchangling iron deposit. In *Chinese iron ore deposit* (pp. 279–284). Beijing: Metallurgical Industry Press. (in Chinese)

Chung, D., Zhou, M. F., Gao, J. F., & Chen, W. T. (2015). In-situ LA–ICP-MS trace elemental analyses of magnetite: The late Palaeoproterozoic Sokoman Iron Formation in the Labrador Trough, Canada. *Ore Geology Reviews*, *65*, 917–928.

Dai, Y. P., Zhang, L. C., Zhu, M. T., Wang, C. L., Liu, L., & Xiang, P. (2014). The composition and genesis of the Mesoarchean Dagushan banded iron formation (BIF) in the Anshan area of the North China Craton. *Ore Geology Reviews*, *63*, 353–373.

Dare, S. A. S., Barnes, S. J., & Beaudoin, G. (2012). Variation in trace element content of magnetite crystallized from a fractionating sulfide liquid, Sudbury, Canada: Implications for provenance discrimination. *Geochimica et Cosmochimica Acta*, *88*, 27–50.

Dupuis, C., & Beaudoin, G. (2011). Discriminant diagrams for iron oxide trace element fingerprinting of mineral deposit types. *Mineralium Deposita*, *46*, 319–335.

Gross, G. A. (1980). A classification of iron formations based on depositional environment. *Canadian Mineralogist*, *18*, 215–222.

Guan, G. Y. (1961). The significance of metamorphism in the genesis of high-grade iron ore. *Acta Geologica Sinica*, *41*, 65–76. (in Chinese with Russian abstract)

Holdaway, M. (2000). Application of new experimental and garnet Margules data to the garnet-biotite geothermometer. *American Mineralogist*, *85*, 881–892.

Huang, X. W., Zhou, M. F., Qi, L., Gao, J. F., & Wang, Y. W. (2013). Re-Os isotopic ages of pyrite and chemical composition of magnetite from the Cihai magmatic-hydrothermal Fe deposit, NW China. *Mineralium Deposita*, *48*, 925–946.

Huang, X. W., Gao, J. F., Qi, L., & Zhou, M. F. (2015). In-situ LA-ICP-MS trace elemental analyses of magnetite and Re–Os dating of pyrite: The Tianhu hydrothermally remobilized sedimentary Fe deposit, NW China. *Ore Geology Reviews*, *65*, 900–916.

James, H. L. (1954). Sedimentary facies of iron-formation. *Economic Geology*, *49*, 235–293.

Li, S. B. (1979). A contribution to the genesis of rich magnetite deposit of the Gongchangling type: In the light of graphite discovery in it. *Geochimica*, *8*, 170–177. (in Chinese with English abstract)

Li, S. G. (1982). Geochemical model for the genesis of the Gongchangling rich magnetite deposit in China. *Geochimica*, *11*, 113–121. (in Chinese with English abstract)

Li, X. H., & Li, Q. L. (2016). Major advances in microbeam analytical techniques and their applications in Earth Science. *Science Bulletin*, *61*, 1785–1787.

Li, B. C., & Shi, J. X. (1979). Research on the composition of gas-liquid inclusions and its application. *Geology and Prospecting*, *3*, 16–21.

Li, B. L., Li, X. M., Cui, X. F., & Wang, Z. L. (1977). Fluid inclusions thermometry of mineral from Gongchangling No.2 mining area. *Journal of University of Science and Technology of China*, *7*, 96–103. (in Chinese)

Li, S. G., Zhi, C. X., Chen, J. F., Wang, J. X., & Deng, Y. Y. (1983). Origin of graphites in early Precambrian banded iron formation in Anshan, China. *Geochimica*, *12*, 162–169. (in Chinese with English abstract)

Li, H. M., Liu, M. J., Li, L. X., Yang, X. Q., Chen, J., Yao, L. D., … Yao, T. (2012). Geology and geochemistry of the marble in the Gongchangling iron ore deposit in Liaoning Province and their metallogenic significance. *Acta Petrologica Sinica*, *28*, 3497–3512. (in Chinese with English abstract)

Li, H. M., Zhang, Z. J., Li, L. X., Zhang, Z. C., Chen, J., & Yao, T. (2014). Types and general characteristics of the BIF-related iron deposits in China. *Ore Geology Reviews*, *57*, 264–287.

Li, S. Z., Li, X. Y., Dai, L. M., Liu, X., Zhang, Z., Zhao, S. J., … Zhang, G. W. (2015a). Precambrian geodynamics (VI): Formation of North China Craton. *Earth Science Frontiers*, *22*(6), 77–96. (in Chinese with English abstract)

Li, H. M., Yang, X. Q., Li, L. X., Zhang, Z. C., Liu, M. J., Yao, T., & Chen, J. (2015b). Desilicification and iron activation–reprecipitation in the high-grade magnetite ores in BIFs of the Anshan-Benxi area, China: Evidence from geology, geochemistry and stable isotopic characteristics. *Journal of Asian Earth Sciences*, *113*, 998–1016.

Li, S. Z., Zhao, G. C., & Sun, M. (2016). Paleoproterozoic amalgamation of the North China Craton and the assembly of the Columbia supercontinent. *Chinese Science Bulletin*, *61*, 919–925. (in Chinese with English abstract)

Liu, P. (1985). Source of Au in metamorphic hydrothermal fluid. *Geology ang Prospecting*, *21*, 1–5.

Liu, J., & Jin, S. Y. (2010). Genesis study of magnetite-rich ore in Gongchangling iron deposit, Liaoning. *Geoscience*, *24*, 80–88. (in Chinese with English abstract)

Liu, Y. S., Hu, Z. C., Gao, S., Günther, D., Xu, J., Gao, C. G., & Chen, H. H. (2008). In situ analysis of major and trace elements of anhydrous minerals by LA-ICP-MS without applying an internal standard. *Chemical Geology*, *257*, 34–43.

Liu, P. P., Zhou, M. F., Chen, W. T., Gao, J. F., & Huang, X. W. (2015). In-situ LA-ICP-MS trace elemental analyses of magnetite: Fe–Ti–(V) oxide-bearing mafic–ultramafic layered intrusions of the Emeishan Large Igneous Province, SW China. *Ore Geology Reviews*, *65*, 853–871.

Nadoll, P., Mauk, J. L., Hayes, T. S., Koenig, A. E., & Box, S. E. (2012). Geochemistry of magnetite from hydrothermal ore deposits and host rocks of the Mesoproterozoic Belt Supergroup, United States. *Econmic Geology*, *107*, 1275–1292.

Nadoll, P., Angerer, T., Mauk, J. L., French, D., & Walshe, J. (2014). The chemistry of hydrothermal magnetite: A review. *Ore Geology Reviews*, *61*, 1–32.

Powell, R., Holland, T., & Worley, B. (1998). Calculating phase diagrams involving solid solutions via non-linear equations, with examples using THERMOCALC. *Journal of Metamorphic Geology*, *16*, 577–588.

Shi, J. X., & Li, B. C. (1980). Origin of rich magnetite ores in the Gongchangling area as evidenced by fluid inclusion studies from the Anshan-Benxi region, Northeast China. *Geochimica*, *9*, 43–53. (in Chinese with English abstract)

Song, B., Nutman, A. P., Liu, D., & Wu, J. (1996). 3800 to 2500 Ma crustal evolution in the Anshan area of Liaoning Province, northeastern China. *Precambrian Research*, *78*, 79–94.

Sun, X. H., Zhu, X. Q., Tang, H. S., Zhang, Q., & Luo, T. Y. (2014). The Gongchangling BIFs from the Anshan–Benxi area, NE China: Petrological–geochemical characteristics and genesis of high-grade iron ores. *Ore Geology Reviews*, *60*, 112–125.

Tang, H. S., Chen, Y. J., Santosh, M., Zhong, H., Wu, G., & Lai, Y. (2013a). C-O isotope geochemistry of the Dashiqiao magnesite belt, North China Craton: Implications for the Great Oxidation Event and ore genesis. *Geological Journal*, *48*, 467–483.

Tang, H. S., Chen, Y. J., Santosh, M., Zhong, H., & Yang, T. (2013b). REE geochemistry of carbonates from the Guanmenshan Formation, Liaohe Group, NE Sino-Korean Craton: Implications for seawater compositional change during the Great Oxidation Event. *Precambrian Research*, *227*, 316–336.

Thorne, W. S., Hagemann, S. G., Webb, A., & Clout, J. (2008). Banded iron formation-related iron ore deposits of the Hamersley Province, Western Australia. In S. G. Hagemann, C. A. Rosière, J. Gutzmer, & N. J. Beukes (Eds.), *Banded iron formation-related high-grade iron ore* (pp. 197–222). Colorado: Society of Economic Geologists.

Verlaguet, A., Brunet, F., Goffé, B., & Murphy, W. M. (2006). Experimental study and modeling of fluid reaction paths in the quartz–kyanite ± muscovite–water system at 0.7 GPa in the 350–550°C range: Implications for Al selective transfer during metamorphism. *Geochimica et Cosmochimica Acta*, *70*, 1772–1788.

Wan, Y. S. (1993). *Formation and evolution of the iron-bearing rock series of Gongchangling area, Liaoning Province* (pp. 1–108). Beijing: Beijing Science and Technology Press. (in Chinese)

Wan, Y. S., Dong, C. Y., Xie, H. Q., Wang, S. J., Song, M. C., Xu, Z. Y., … Liu, D. Y. (2012). Formation ages of early Precambrian BIFs in the North China Craton: SHRIMP zircon U-Pb dating. *Acta Geologica Sinica*, *86*, 1447–1478. (in Chinese with English abstract)

Wang, E. D., Xia, J. M., Fu, J. F., Jia, S. S., & Men, Y. K. (2014). Formation mechanism of Gongchangling high-grade magnetite deposit hosted in Archean BIF, Anshan-Benxi area, Northeastern China. *Ore Geology Reviews*, *57*, 308–321.

Wu, C. M., & Cheng, B. H. (2006). Valid garnet–biotite (GB) geothermometry and garnet–aluminum silicate–plagioclase–quartz (GASP) geobarometry in metapelitic rocks. *Lithos*, *89*, 1–23.

Wu, C. M., Zhang, J., & Ren, L. D. (2004). Empirical garnet–biotite–plagioclase–quartz (GBPQ) geobarometry in medium-to high-grade metapelites. *Journal of Petrology*, *45*, 1907–1921.

Zhai, M. G., & Santosh, M. (2011). The early Precambrian odyssey of the North China Craton: A synoptic overview. *Gondwana Research*, *20*, 6–25.

Zhai, M. G., & Windley, B. F. (1990). The Archaean and early Proterozoic banded iron formations of North China: Their characteristics, geotectonic relations, chemistry and implications for crustal growth. *Precambrian Research*, *48*, 267–286.

Zhai, M. G., Sills, J. D., & Windley, B. F. (1990a). Metamorphic mineral and metamorphism of the Anshan Group in Anshan-Benxi area, Liaoning. *Acta Petrologica et Mineralogica*, *9*, 148–158. (in Chinese with English abstract)

Zhai, M. G., Windley, B. F., & Sills, J. D. (1990b). Archaean gneisses, amphibolites and banded iron-formations from the Anshan area of Liaoning Province, NE China: Their geochemistry, metamorphism and petrogenesis. *Precambrian Research*, *46*, 195–216.

Zhang, L. C., Zhai, M. G., Wan, Y. S., Guo, J. H., Dai, Y. P., Wang, C. L., & Liu, L. (2012a). Study of Precambrian BIF-iron deposits in North China Craton: Progress and questions. *Acta Petrologica Sinica*, *28*, 3431–3445. (in Chinese with English abstract)

Zhang, L. C., Zhai, M. G., Zhang, X. J., Xiang, P., Dai, Y. P., Wang, C. L., & Pirajno, F. (2012b). Formation age and tectonic setting of the Shirengou Neoarchean banded iron deposit in eastern Hebei Province: Constraints from geochemistry and SIMS zircon U–Pb dating. *Precambrian Research*, *222-223*, 325–338.

Zhao, B., & Li, T. J. (1980). A preliminary study on the mechanism and physico-chemical conditions of the formation of the Gongchangling rich iron deposit. *Geochimica*, *9*, 333–344. (in Chinese with English abstract)

Zhao, G. C., & Zhai, M. G. (2013). Lithotectonic elements of Precambrian basement in the North China Craton: Review and tectonic implications. *Gondwana Research*, *23*, 1207–1240.

Zhao, B., Wang, S. Y., & Li, T. J. (1979). The origin of migmatite granite and its relationship with iron deposit: An experimental study. *Geochimica*, *8*, 211–221. (in Chinese with English abstract)

Zhao, G. C., Sun, M., Wilde, S. A., & Li, S. Z. (2005). Late Archean to Paleoproterozoic evolution of the North China Craton: Key issues revisited. *Precambrian Research*, *136*, 177–202.

Zhou, S. T. (1987). The petrochemical study of the Archean banded iron deposit in Anshan-Benxi district, Liaoning Province. *Bulletin of the Chinese Academy of Geological Sciences*, *16*, 139–153. (in Chinese with English abstract)

Zhou, S. T. (1994). *Geology of banded iron formations in Anshan-Benxi area* (pp. 1–278). Beijing: Geological Publishing House. (in Chinese)

Zhou, S. T. (1997). The research progress and forecasting of Chinese Archean banded iron formation. *Geology and Prospecting*, *33*, 1–7. (in Chinese with English abstract)

Zhou, Z. J., Tang, H. S., Chen, Y. J., & Chen, Z. L. (2017). Trace elements of magnetite and iron isotopes of the Zankan iron deposit, westernmost Kunlun, China: A case study of seafloor hydrothermal iron deposits. *Ore Geology Reviews*, *80*, 1191–1205.

SUPPORTING INFORMATION

Additional Supporting Information may be found online in the supporting information tab for this article.

How to cite this article: Sun X, Zhu X, Tang H, Luan Y. In situ LA-ICP-MS trace element analysis of magnetite from the late Neoarchean Gongchangling BIFs, NE China: Constraints on the genesis of high-grade iron ore. *Geological Journal*. 2018;53(S1):8–20. https://doi.org/10.1002/gj.3004